Supporting Information

Kim and Allen 10.1073/pnas.1110735108

SI Text

Detailed Methods. ***Simulations.*** The fully atomistic molecular dynamics (MD) simulation system is shown in Fig. 1 of the main text. The system includes 115 lipid molecules (65 in the bottom and 50 in the top leaflet), 7,630 water molecules, and ~150 mL KCl, corresponding to 15 K^+ and 23 Cl^- ions (for electroneutrality), totaling ~43,770 atoms. The CHARMM program (1) (version 32), with the PARAM27 force field (2) [lipids (3, 4) and TIP3P water (5)], including CMAP corrections (6) have been used for all simulations.

Electrostatics were computed using the Particle Mesh Ewald algorithm (7), a 12 Å Lennard-Jones truncation, and bonds to H atoms were maintained with the SHAKE algorithm (8). Simulations were performed under constant normal pressure (1 atm) with an extended Lagrangian (9, 10) and temperature (330 K, above the dipalmitoylphosphatidylcholine, DPPC, gel phase transition temperature) was controlled by a Nose-Hoover thermostat (11, 12). Hexagonal periodic boundary conditions with *xy*-translation length of ~77 Å and average height of ~90 Å was preserved with piston mass of 750 amu) and collision frequency 5 ps^{-1}. To prevent protein drift in the *xy* plane, a cylindrical constraint of 5 kcal/mol/$Å^2$ was applied to the center of mass (COM) of KcsA, and a 5 kcal/mol/$Å^2$ planar constraint in *z*-direction was also applied to the lipid membrane COM (neither constraint having any effect on results).

It is known that CHARMM describes hydration free energies well without any force field modification (13, 14), yet ion-carbonyl Lennard-Jones parameters have been modified to ensure correct solvation in N-methylacetamide (NMA) (14–16). Absolute free energies of K^+ solvation in water and NMA are −79.6 kcal/mol (13) and −83.2 kcal/mol, respectively (17, 18), while those for Na^+ are −98.1 and −99.9 kcal/mol (19).

It has been previously reported that the carbonyl groups of Val76 may flip away in the wild-type KcsA selectivity filter during MD simulations (14, 20–22), possibly associated with C-type inactivation (22–24). In order to only capture conducting conformations, a weak harmonic dihedral constraint with force constant 0.0030 kcal/mol/ deg^2, centered on −90°, was applied to ψ dihedral angles of each Val76.

Free energy perturbation. Free energy perturbation calculations for individual sites involved multiple biased simulations. The ion was either held near the crystallographic K^+ site centered at the COM of eight carbonyls, or in the plane of the four carbonyls. Planar harmonic potentials of 60 kcal/mol/$Å^2$, 10 kcal/mol/$Å^2$, and 2.5 kcal/mol/$Å^2$, were used, allowing root mean square fluctuations of ~0.1, 0.25, and 0.5 Å, respectively. For unconstrained $\Delta\Delta G$ calculations, simulations were carried out with the ion of interest free to move, but with flat-bottom constraints applied to ensure the S0 ion stays within the selectivity filter region ($-8 < z < 10$ Å).

Initially, free energy perturbation (FEP) (25, 26) calculations were performed via Thermodynamic Integration (TI) (27) or Weighted Histogram Analysis Method (WHAM) (28, 29), using a linear coupling scheme with 11 windows from $\lambda = 0$ to 1, each of which runs for 0.25 ns for equilibration, followed by 0.5 ns for production. To sample each binding site, we carried out a total of six (for S0 or S4) or nine (for S1, S2 or S3) constrained simulations, for each of the 11 windows: i.e., in each of the lower plane, cage, or upper plane of the site using constraints of three different strengths (2.5, 10, 60 kcal/mol/$Å^2$, corresponding to root mean square fluctuation values of 0.5, 0.25, and 0.1 Å, respectively). In bulk solution, six independent free energy perturbations were carried out, spanning 27.5–30 Å in 0.25 Å steps, apart, held with 10 kcal/mol/$Å^2$, near the edge of simulation box.

For individual sites we have also calculated relative free energies using Bennett Overlapping Histograms (BOH) (30–32). In this method, one seeks an overlap of normalized histograms (probability distributions) of energy difference, $\hat{H}_{K^+}(\Delta U)$ and $\hat{H}_{Na^+}(\Delta U)$, obtained from the K^+ ($\lambda = 0$) or Na^+ ($\lambda = 1$) simulations respectively, such that

$$\frac{\hat{H}_{Na^+}(\Delta U)}{\hat{H}_{K^+}(\Delta U)} = e^{-(\Delta U - \Delta G_{K^+ \to Na^+})/kT}, \qquad \textbf{[S1a]}$$

where k is Boltzmann's constant, or, equivalently,

$$-kT \ln \frac{\hat{H}_{Na^+}(\Delta U)}{\hat{H}_{K^+}(\Delta U)} = \Delta U - \Delta G_{K^+ \to Na^+} \qquad \textbf{[S1b]}$$

seeking the perturbation energy, ΔU, where the ratio of densities equals unity (i.e., $\Delta U \to \Delta G$). Following Bennett (30–32), the free energy difference, ΔG, is estimated from the plateau of difference between two functions,

$$\begin{aligned} g_{K^+}(\Delta U) &= \ln \hat{H}_{K^+}(\Delta U) - \frac{1}{2}\beta \Delta U; \\ g_{Na^+}(\Delta U) &= \ln \hat{H}_{Na^+}(\Delta U) - \frac{1}{2}\beta \Delta U \end{aligned} \qquad \textbf{[S2a]}$$

such that,

$$g_{Na^+}(\Delta U) - g_{K^+}(\Delta U) = \beta \Delta G \qquad \textbf{[S2b]}$$

over the energy regions where two probability distributions (or histograms) overlap. We also applied the Bennett-Hummer Least Square (BHLS) approach (33, 34), where free energy difference is determined by least square plot of Eq. **S1b**, whose slope and intersection are kT and $-\Delta G/kT$, respectively. Though less statistically reliable, the free energy difference can be estimated by the energy difference at the histogram intersection (HI) (35).

One can also see ΔG emerge by rearranging Eq. **S1a** (removing subscript $K^+ \to Na^+$ for brevity)

$$\hat{H}_{K^+}(\Delta U) e^{-\Delta U/kT} = \hat{H}_{Na^+}(\Delta U) e^{-\Delta G/kT} \qquad \textbf{[S3]}$$

and integrating over energy to find,

$$\begin{aligned} \int \hat{H}_{K^+}(\Delta U) e^{-\Delta U/kT} d\Delta U &= e^{-\Delta G/kT} \int \hat{H}_{Na^+}(\Delta U) d\Delta U \\ &= e^{-\Delta G/kT}. \end{aligned} \qquad \textbf{[S4]}$$

Improved measures can be obtained by using the Bennett Acceptance Ratio (BAR) method (30). BAR is capable of achieving the smallest error for alchemical mutations and solvation free energies in the large sampling limit (36). Optimal estimation of free energy difference emerges from the following iterative equation with unnormalized histograms of energy difference $H_{K^+,Na^+}(\Delta U)$,

$$\Delta G = \mathrm{kT}\ln\frac{\sum_{\Delta U} H_{\mathrm{K}^+}(\Delta U) f(\Delta U - \Delta G - M)}{\sum_{\Delta U} H_{\mathrm{Na}^+}(\Delta U) f(-\Delta U + \Delta G + M)} + \Delta G, \qquad \textbf{[S5]}$$

where $M = kT\ln n_{\mathrm{Na}}/n_{\mathrm{K}}$ with n_{K} and n_{Na} being the number of MD simulation steps in each state, and where f is the Fermi function, $f(x) = 1/(1+\exp(x/\mathrm{kT}))$. We have solved Eq. **S5** in a iterative manner with the criterion for convergence (30),

$$\sum_{\Delta U} H_{\mathrm{Na}^+}(\Delta U) f(-\Delta U + \Delta G + M) = \sum_{\Delta U} H_{\mathrm{K}^+}(\Delta U) f(\Delta U - \Delta G - M). \qquad \textbf{[S6]}$$

To overcome poorly overlapping histograms that arise when ions are not restrained, we have shown that they can instead be built up from trajectories sampled during the Umbrella Sampling (US) simulations, detailed in the next section. E.g.,

$$H_{\mathrm{K}^+}(\Delta U) = \int_{z_0}^{z_1} H_{\mathrm{K}^+}(\Delta U|z)\hat{\rho}_{\mathrm{K}^+}(z)dz, \qquad \textbf{[S7]}$$

where $H_{\mathrm{K}^+}(\Delta U|z)$ is the conditional biased histogram of energy difference ΔU given a particular value of z, obtained by analysis of US trajectories, and $\hat{\rho}_{\mathrm{K}^+}(z)$ is the normalized histogram (probability density) as function of position, obtained from the potential of mean force (PMF, $W_{\mathrm{K}^+}(z)$), as done for Na^+, via

$$\hat{\rho}_{\mathrm{K}^+}(z) = \frac{e^{-W_{\mathrm{K}^+}(z)/\mathrm{kT}}}{\int_{z_0}^{z_1} e^{-W_{\mathrm{K}^+}(z)/\mathrm{kT}}dz}; \qquad \hat{\rho}_{\mathrm{Na}^+}(z) = \frac{e^{-W_{\mathrm{Na}^+}(z)/\mathrm{kT}}}{\int_{z_0}^{z_1} e^{-W_{\mathrm{Na}^+}(z)/\mathrm{kT}}dz}. \qquad \textbf{[S8]}$$

By substitution of Eq. **S7** into Eq. **S5** and Eq. **S6** using BAR with US (BAR-US), as done for our main results in Table 1 of the main text, the problems associated with an endpoint calculation of the FEP for the $\mathrm{K}^+ \rightarrow \mathrm{Na}^+$ transition disappear, because the configurational space for both the K^+ and Na^+ ions is well sampled via US, assuming the coordinate (z) is a good coordinate for mapping configurational space (3N-D) into energy difference space [one-dimensional (1D)] via $H_{\mathrm{K}^+,\mathrm{Na}^+}(\Delta U|z)$ in Eq. **S7**.

Eq. **S7** has also been used within Eq. **S3** to estimate the free energy difference using the methods of BOH-US and BHLS-US. In addition, Eq. **S7** is easily extended to multidimensional US simulations. For example, we have used the three-dimensional (3D) free energy surface (see below) as a function of the position of the S2 ion (z_2) and the relative positions of ion 1 and ion 3 to this ion, in a S0/S2/S4 configuration,

$$H_{\mathrm{K}^+}(\Delta U) = \iiint H_{\mathrm{K}^+}(\Delta U|z_2,\Delta z_{12},\Delta z_{13})\hat{\rho}_{\mathrm{K}^+}(z_2,\Delta z_{12},\Delta z_{13})dz_2 d\Delta z_{12} d\Delta z_{13}. \qquad \textbf{[S9]}$$

This equation was used with Eq. **S6** and Eq. **S7** to evaluate free energy difference across S2 (BAR-3D in Table 1).

Free energy profiles. By combining the trajectories from biased simulations with dedicated US (37) simulations, 1D PMFs have been computed across S0, S1, S2, S3, and S4 sites. We simulated 14–16 additional US windows for s1, s2, and s3, maintained with a force constant of 10 kcal/mol/Å^2, spanning the lower plane, cage, and upper plane of a site in 0.25 Å steps, with each window run for 1–1.5 ns and combined with the other 6–9 windows within a single WHAM analysis. The chosen reaction coordinate was the z-position of the ion relative to the z-component of the COM of the eight carbonyl groups of the site, which was then transformed into a common coordinate (relative to the COM of the entire filter) by adding the z-component of COM of the site. For some extreme positions of the ion being studied, other ions may tend to move (see *The Challenge of Multi-ion Movements* of the main text), but have been kept from escaping the filter by applying steep flat-bottom potentials. To stop an ion in S4 leaving to the cavity, the lower bound was placed at $z = -8$ Å (results were found to be independent of the position of this constraint when moved by 0.5 Å; not shown), while to stop an ion in S0 escaping to the outside, an upper bound was placed at $z = 10$ Å.

Observations of multiple ion movements led us to carry out two-dimensional (2D) and 3D US to compute the free energy surface governing the movements of S1 and S3 K^+ and Na^+ ions, as well as for the movements of S0, S2, and S4 ions where the S2 ion was either a K^+ or a Na^+ ion. For the case of the 2D free energy surface for S1/S3 movements, nine umbrellas were used for S1(S3), spanning 3 to 7 Å (−4.5 to −0.5 Å) and six for the S1–S3 distance, spanning 4.5 to 7.0 Å ($9\times6 = 54$ in total) in 0.5 Å increments, using a force constant of 10 kcal/mol/Å^2. In the case of the 3D free energy surface as function of S0, S2, and S4 ions, six umbrellas were used for the S0 ion, relative to the S2 ion, spanning 4.5–7.0 Å, 9 for the S2 ion spanning −0.75–3.25, and six for the S4–S2 distance spanning 4.5–7.0 in 0.5 Å increments (a total of $9\times6\times6 = 324$ windows), using a force constant of 10 kcal/mol/Å^2. (Note: to illustrate the sampling challenges in Fig. 4, US for the S0 ion was carried out not only for K^+ and Na^+ ions, but for all partial coupling parameter values, $\lambda = 0$–1 in 0.1 steps). Once the multi-D free energy surface was obtained, an improved 1D free energy profile for the S1, S3, or S2 ion (as a K^+ or Na^+ ion) was obtained simply by integration out of the multi-D density. E.g., for K^+ in S2,

$$\rho_{\mathrm{K}^+}(z_2) = e^{-W_{\mathrm{K}^+}(z_2)/\mathrm{kT}} = \iint e^{-W_{\mathrm{K}^+}(z_2,\Delta z_{12},\Delta z_{23})/\mathrm{kT}} d\Delta z_{12} d\Delta z_{23}, \qquad \textbf{[S10]}$$

where Δz_{12} and Δz_{23} are the relative positions of ions above and below the S2 ion. The relative shift between K^+ and Na^+ profiles was determined by

$$W(z) = W'(z) + \Delta G + \mathrm{kT}\ln\frac{\hat{\rho}^{\max}_{\mathrm{K}^+}}{\hat{\rho}^{\max}_{\mathrm{Na}^+}}, \qquad \textbf{[S11]}$$

where $W'(z)$ and $W(z)$ are the PMF before and after the shift, ΔG is the net free energy difference over the site (from Table 1), and where only the maximum values of the normalized densities are needed for the last term.

To estimate the time scales of barrier crossings in individual free energy profiles, we have computed Kramer's rates (38), assuming an approximate ionic diffusion coefficient (D) of 0.01 Å^2/ps inside the channel, similar to previous estimates (20, 39)

$$\mathrm{rate} = \frac{D\sqrt{K_b K_w}}{2\pi k_b T}\exp(-\Delta W/\mathrm{kT}), \qquad \textbf{[S12]}$$

where K_b and K_w are the curvatures at the barrier and well, respectively, and ΔW is the free energy difference between the barrier and the well. Curvatures were evaluated by fitting 11 points near the extrema with quadratics.

We have also carried out 1D US simulations to calculate the PMFs of K^+ and Na^+ binding from the outside of the selectivity filter that is occupied by either K^+ or Ba^{2+} ions, as explained in the main text. A total of 23 windows, spanning $4.5 < z < 16$ Å, for K^+ or Ba^{2+} were used to sample the pathway for the external

ion, in 0.5 Å increments, with a force constant of 10 kcal/mol/Å^2. Using these PMFs, we have computed dissociation constants, K_D, for the binding of K^+ or Na^+ to the filter in the presence of K^+ or Ba^{2+} ions from the expression (40)

$$K_D{}^{-1} = \pi R^2 \int_{z_{\min}}^{z_{\max}} dz \exp(-W(z)/k_bT), \qquad \textbf{[S13]}$$

where, R (5 Å in the present study) is the radius of a steep cylindrical flat-bottom potential oriented normal to the reaction coordinate (z), with the binding region defined between $z_{\min} = 4.5$ Å and $z_{\max} = 9.0$ Å. The reference for the PMFs in these estimates was taken as the minimum of Na^+ PMF (close to the minimum of K^+ PMF) outside of selectivity filter.

Comparison of combined FEP with US and BAR-US approaches. The net or overall FEP for the transformation from K^+ to Na^+ over a region in coordinate z, can be deduced from the free energies of the ions as a function of position

$$e^{-G^{\text{overall}}_{K^+}/\text{kT}} = e^{-G_{K^+}(z_0)/\text{kT}} \int_{z_0}^{z_1} e^{-W_{K^+}(z)/\text{kT}} dz \qquad \textbf{[S14a]}$$

$$e^{-G^{\text{overall}}_{Na^+}/\text{kT}} = e^{-G_{Na^+}(z_0)/\text{kT}} \int_{z_0}^{z_1} e^{-W_{Na^+}(z)/\text{kT}} dz, \qquad \textbf{[S14b]}$$

where z_0 is a chosen reference position (e.g., the cage site), the PMFs, $W(z)$, and have already been expressed relative to this position ($W(z) = G(z) - G(z_0)$). Thus

$$e^{-\Delta G^{\text{overall}}_{K^+\to Na^+}/\text{kT}} = e^{-\Delta G_{K^+\to Na^+}(z_0)/\text{kT}} \frac{\int_{z_0}^{z_1} e^{-W_{Na^+}(z)/\text{kT}} dz}{\int_{z_0}^{z_1} e^{-W_{K^+}(z)/\text{kT}} dz} \qquad \textbf{[S15]}$$

i.e., the relative thermodynamic stability of Na^+, relative to K^+, within a region between z_0 and z_1 (spanning, for instance, the cage, and planes of a site) can be obtained from the PMFs of the individual ions, given an estimate of $\Delta G_{K^+}(z_0)$ at one position from a TI, WHAM, or Bennett calculation. We have illustrated this approximate calculation in the main text; approximate because in practice we employed an estimate from a distribution near the cage, whereas $\Delta G(z_0)$ in Eq. **S15** refers to a single position.

Now consider the Bennett histogram approaches that utilize endpoint, K^+ ($\lambda = 0$) and Na^+ ($\lambda = 1$), simulations only. For the purpose of this illustration, the simple BOH formalism of Eq. **S1a** will be considered, in combination with US simulations Eq. **S7**, which leads to

$$\frac{\int_{z_0}^{z_1} H_{Na^+}(\Delta U|z)\hat{\rho}_{Na^+}(z)dz}{\int_{z_0}^{z_1} H_{K^+}(\Delta U|z)\hat{\rho}_{K^+}(z)dz} = e^{-(\Delta U - \Delta G)/\text{kT}}. \qquad \textbf{[S16]}$$

Rearranging and integrating over energy (as done to find Eq. **S4**), and using the fact that the histograms have been normalized, one can easily show, somewhat trivially

$$\int_{z_0}^{z_1} dz \hat{\rho}_{K^+}(z) e^{-\Delta G(z)/\text{kT}} = e^{-\Delta G/\text{kT}}. \qquad \textbf{[S17]}$$

Using Eq. **S8** for K^+ we have

$$\frac{\int_{z_0}^{z_1} dz e^{-W_{K^+}(z)/\text{kT}} e^{-\Delta G(z)/\text{kT}}}{\int_{z_0}^{z_1} e^{-W_{K^+}(z)/\text{kT}} dz} = e^{-\Delta G/\text{kT}} \qquad \textbf{[S18]}$$

or, using the fact that the PMF, W, has already been expressed relative to position z_0,

$$\begin{aligned}
&\frac{\int_{z_0}^{z_1} dz e^{-[G_{K^+}(z) - G_{K^+}(z_0)]/\text{kT}} e^{-[G_{Na^+}(z) - G_{K^+}(z)]/\text{kT}}}{\int_{z_0}^{z_1} dz e^{-W_{K^+}(z)/\text{kT}}} \\
&= \frac{\int_{z_0}^{z_1} dz e^{-[-G_{K^+}(z_0)]/\text{kT}} e^{-[G_{Na^+}(z)]/\text{kT}}}{\int_{z_0}^{z_1} dz e^{-W_{K^+}(z)/\text{kT}}} \\
&= \frac{\int_{z_0}^{z_1} dz e^{-[G_{Na^+}(z_0) - G_{K^+}(z_0)]/\text{kT}} e^{-W_{Na^+}(z)/\text{kT}}}{\int_{z_0}^{z_1} dz e^{-W_{K^+}(z)/\text{kT}}} \\
&= e^{-\Delta G(z_0)/\text{kT}} \frac{\int_{z_0}^{z_1} dz e^{-W_{Na^+}(z)/\text{kT}}}{\int_{z_0}^{z_1} dz e^{-W_{K^+}(z)/\text{kT}}} = e^{-\Delta G/\text{kT}}
\end{aligned} \qquad \textbf{[S19]}$$

just as in Eq. **S15**. Thus, the net thermodynamic stabilities from Eq. **S16** and Eq. **S15** should, in theory, yield the same ΔG quantity, and this has been used as an approximate test of the results. For example, when Eq. **S15** is applied to the PMFs for S2, together with the FEP estimate for the cage from Table 1, the overall/net selectivity of S2 is +1.5 kcal/mol, consistent with the BAR-US result in Table 1 of the main text.

Comparison of FEP and BAR estimates of $\Delta\Delta G$ in individual sites. In Fig. S3 we show, for the case of a cage or plane site in S2, for example, that BAR endpoint and TI/WHAM give consistent results. We have only shown the S2 cage and lower plane site because they are the most significant for the discussion in the main text and represent a typical situation. Reasonable overlap of energy probability distribution was achieved and the BOH-US analysis in Fig. S3 reveals a good plateau in the cage site, as well as for the lower plane site (noting the very small range in energy in the vertical axis) using Eq. **S3** with Eq. **S6** and Eq. **S7**, implying the free energy difference using the method of BOH-US converges well (30–33). The free energy difference obtained by BOH-US is also consistent with those from BAR-US and TI/WHAM.

Comparison of BAR/BOH/BHLS and BAR-US/BOH-US/BULS-US for unconstrained ions. Fig. S6*A* reveals, for the case of the S2 site, that when the ions are not constrained, overlap of histograms is poor, with data collected for 1 ns following a 1 ns period after the Na^+ ion left the S2 cage site (see left box of *A*). As a result, no plateau in the BOH analysis is seen (central box of *A*). However, when combined with US (part *B*), the overlap of histograms is much improved (left box of *B*), and a good plateau in BOH analysis is seen (central box of *B*).

Comments on asymmetries in the binding sites. As discussed in the main text, there are several reasons why the PMF across each cite may not be symmetric. The schematic in Fig. S4 illustrates how the movement of the ions to upper or lower planes may have different consequences for the movement of other ions and water molecules, and subsequent effects on energy.

In the case of the S0 site (in a S0/S2/S4 configuration), only a lower plane exists and the lower plane is thus favored for Na^+. In the case of S1 (in a S1/S3/Cav configuration), the lower plane is again favored for Na^+. Movement to upper plane would require rearrangement of entire column of ions and water or suffer an ion-water interaction loss. Movement to lower plane seems easier as while it is cramped, water may enter from the outside. In the S2 site (in a S0/S2/S4 configuration), the lower site is again favored by Na^+, though the reason is not as obvious. In this case, the K^+ ion in S0 or S4 shifts to the neighboring site when the Na^+ ion moves to a planar site (see *The Challenge of Multi-ion Movements* of the main text). But the movement of K^+ from

S0 to S1 or from S4 to S3 will not involve the same change in free energy. Other sources of asymmetry in S2 are discussed in the main text. For the S3 ion (in S1/S3/Cav configuration), the upper plane is favored by Na^+. Movement to the lower plane would require rearrangement of entire column of ions and water, or suffer cost of lost ion-water interaction. A similar situation (Na^+ favoring the upper plane) also exists for the S4 site, though in this case the lower plane of S4 is different, consisting of hydroxyl rather than carbonyl groups.

Comparison of 1D PMFs emerging from 1, 2, and 3D US. Fig. S5 compares the PMFs calculated from 1D, 2D, and 3D US simulations for sites S1, S2, and S3. For S1 and S3, either just the ion being mutated was sampled via US (1D), or both of those two ions in the filter were sampled via US (2D). For the S2 case, the S2 ion itself was sampled via US (1D), or the S2 ion together with the upper S0 ion (2D), or all three ions, S0, S2, S4 were sampled via US simulations (3D). The PMFs are broadly similar in each case.

Nonconducting filter simulations. When no constraint was applied to maintain a conducting filter configuration, flipping of carbonyl groups was observed in the presence of Na^+ (see upper diagrams of Fig. S7). In this case, the PMF (lower box) reveals that the Na^+ ion actually becomes favored in the deformed "cage" site. The ability of Na^+ to bind either in a plane of carbonyls, or in a cage coordinated by just five of eight carbonyls, has been previously shown for the S1 site (41), yet Fig. S7 reveals the distribution across a site in the event of carbonyl flipping in S2. When this flipping occurs, we obtain a $\Delta\Delta G$ value for the perturbation ($K^+ \rightarrow Na^+$) of $\sim +3$ kcal/mol (ΔG values of -15.4 ± 0.01 kcal/mol with BAR-US, -15.1 ± 1.1 kcal/mol with BOH-US).

1. Brooks BR, et al. (1983) CHARMM: A program for macromolecular energy minimization and dynamics calculations. *Journal of Computational Chemistry* 4:187–217.
2. MacKerell AD, Jr., et al. (1998) All-atom empirical potential for molecular modeling and dynamics studies of proteins. *Journal of Physical Chemistry B* 102:3586–3616.
3. Feller SE, MacKerell AD, Jr. (2000) An improved empirical potential energy function for molecular simulations of phospholipids. *J Phys Chem B* 104:7510–7515.
4. Yin DX, Mackerell AD (1998) Combined ab initio/empirical approach for the optimization of Lennard-Jones parameters. *J Comput Chem* 19:334–348.
5. Jorgensen WL, Chandrasekhar J, Madura JD, Impey RW, Klein ML (1983) Comparison of simple potential functions for simulating liquid water. *J Chem Phys* 79:926–935.
6. Mackerell AD, Jr. (2004) Empirical force fields for biological macromolecules: overview and issues. *J Comput Chem* 25:1584–1604.
7. Darden TA, Pedersen LG (1993) Molecular modeling: an experimental tool. *Environ Health Perspect* 101:410–412.
8. Ryckaert JP, Ciccotti G, Berendsen HJC (1977) Numerical integration of the Cartesian equations of motion of a system with constraints: molecular dynamics of n-Alkanes. *J Comp Phys* 23:327–341.
9. Anderson HCJ (1980) Molecular dynamics simulations at constant pressure and/or temperature. *Chem Phys* 72:2384–2393.
10. Feller SE, Zhang YH, Pastor RW, Brooks BR (1995) Constant pressure molecular dynamics simulation-the Langevin piston method. *J Chem Phys* 103:4613–4621.
11. Hoover WG (1985) Canonical dynamics: equilibrium phase-space distribution. *Phys Rev A* 31:1695–1697.
12. Nose S (1984) A unified formulation of the constant temperature molecular dynamics methods. *J Chem Phys* 81:511–519.
13. Beglov D, Roux B (1994) Finite representation of an infinite bulk system: solvent boundary potential for computer simulations. *J Chem Phys* 100:9050–9063.
14. Bernèche S, Roux B (2001) Energetics of ion conduction through the K+ channel. *Nature* 414:73–77.
15. Allen TW, Andersen OS, Roux B (2006) Ion permeation through a narrow channel: using gramicidin to ascertain all-atom molecular dynamics potential of mean force methodology and biomolecular force fields. *Biophys J* 90:3447–3468.
16. Noskov SY, Roux B (2008) Control of ion selectivity in LeuT: two Na+ binding sites with two different mechanisms. *J Mol Biol* 377:804–818.
17. Noskov SY, Berneche S, Roux B (2004) Control of ion selectivity in potassium channels by electrostatic and dynamic properties of carbonyl ligands. *Nature* 431:830–834.
18. Lamoureux G, Roux B (2006) Absolute hydration free energy scale for alkali and halide ions established from simulations with a polarizable force field. *J Phys Chem B* 110:3308–3322.
19. Thompson AN, et al. (2009) Mechanism of potassium-channel selectivity revealed by Na+ and Li^+ binding sites within the KcsA pore. *Nat Struct Mol Biol* 16:1317–1324.
20. Allen TW, Kuyucak S, Chung SH (2000) Molecular dynamics estimates of ion diffusion in model hydrophobic and KcsA potassium channels. *Biophys Chem* 86:1–14.
21. Shrivastava IH, Tieleman DP, Biggin PC, Sansom MS (2002) K(+) vs. Na(+) ions in a K channel selectivity filter: a simulation study. *Biophys J* 83:633–645.
22. Berneche S, Roux B (2005) A gate in the selectivity filter of potassium channels. *Structure* 13:591–600.
23. Yellen G (1998) The moving parts of voltage-gated ion channels. *Q Rev Biophys* 31:239–295.
24. Cuello LG, Jogini V, Cortes DM, Perozo E (2010) Structural mechanism of C-type inactivation in K+ channels. *Nature* 466:203–208.
25. Zwanzig RW (1954) High temperature equation of state by a perturbation method: I. Nonpolar gases. *Chem Phys* 22:1420–1426.
26. Kollman P (1993) Free energy calculations: applications to chemical and biochemical phenomena. *Chem Rev* 93:2395–2417.
27. Kirkwood JG (1935) Statistical mechanics of fluid mixtures. *J Chem Phys* 3:300–313.
28. Kumar S, Bouzida D, Swendsen RH, Kollman PA, Rosenberg JM (1992) The weighted histogram analysis method for free-energy calculations on biomolecules. I. The method. *J Comput Chem Rev* 13:1011–1021.
29. Roux B (1995) The calculation of the potential of mean force using computer simulations. *Comp Phys Comm* 91:1–8.
30. Bennett CH (1976) Efficient estimation of free energy differences from Monte Carlo Data. *J Comput Phys* 22:245–268.
31. Frenkel D, Smit B (2002) *Understanding molecular simulation: from algorithms to applications.* (Academic Press, San Diego).
32. Pohorille A, Jarzynski C, Chipot C (2010) Good practices in free-energy calculations. *J Phys Chem B* 114:10235–10253.
33. Rasaiah JC, Hummer G, Noworyta JP (2001) Water conduction through the hydrophobic channel of a carbon nanotube. *Nature* 414:188–190.
34. Pratt LR, Hummer G, Garcia AE (1995) Hydration free energy of water. *J Chem Phys* 99:14188–14194.
35. Collin D, et al. (2005) Verification of the Crooks fluctuation theorem and recovery of RNA folding free energies. *Nature* 437:231–234.
36. Shirts MR, Bair E, Hooker G, Pande VS (2003) Equilibrium free energies from nonequilibrium measurements using maximum likelihood methods. *Phys Rev Lett* 91:140601.
37. Torrie GM, Valleau JP (1977) Nonphysical sampling distributions in Monte Carlo free-energy estimation: umbrella sampling. *J Comput Phys* 23:187–199.
38. Crouzy S, Woolf TB, Roux B (1994) A molecular dynamics study of gating in dioxolane-linked gramicidin A channels. *Biophys J* 67:1370–1386.
39. Mamonov AB, Kurnikova MG, Coalson RD (2006) Diffusion constant of K+ inside Gramicidin A: a comparative study of four computational methods. *Biophysical Chemistry* 124:268–278.
40. Allen TW, Andersen OS, Roux B (2004) Energetics of ion conduction through the gramicidin channel. *Proc Nat Acad Sci USA* 101:117–122
41. Miloshevsky GV, Jordan PC (2008) Conformational changes in the selectivity filter of the open-state KcsA channel: an energy minimization study. *Biophys J* 95:3239–3251.

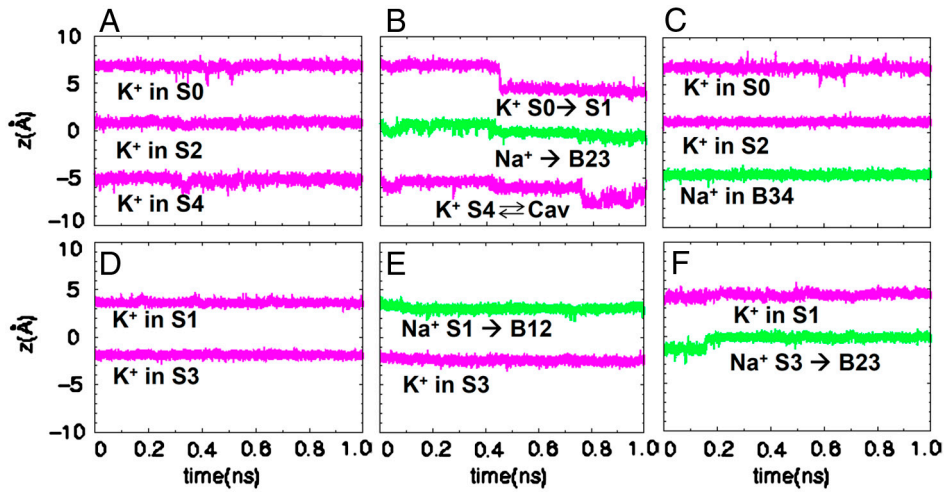

Fig. S1. Unconstrained sample ion trajectory time series: Time series of K^+ and Na^+ ions from unconstrained simulations within the S0/S2/S4 (*A*,*B*,*C*) and S1/S3/Cav configurations (*D*,*E*,*F*). K^+ ions remain in their respective crystallographic cage positions, except for (*B*) where K^+ left for a adjacent cage site (S1) following a transformation of K^+ to Na^+ in S2. In contrast, Na^+ ions always leave the cage sites for their adjacent plane sites. The time series reveal that Na^+ in S2 (*B*) fluctuated between the cage and plane in the first ~500 ps, after which it moved to the plane site, which explains slow convergence of unconstrained FEP in the S2 site; in fact FEP in S2 doesn't converge up to 2 ns. However, Na^+ in S4 (*F*) left in its cage site from the very beginning of the simulations (<50 ps), which explains fast convergence of FEP within 100 ps in that case.

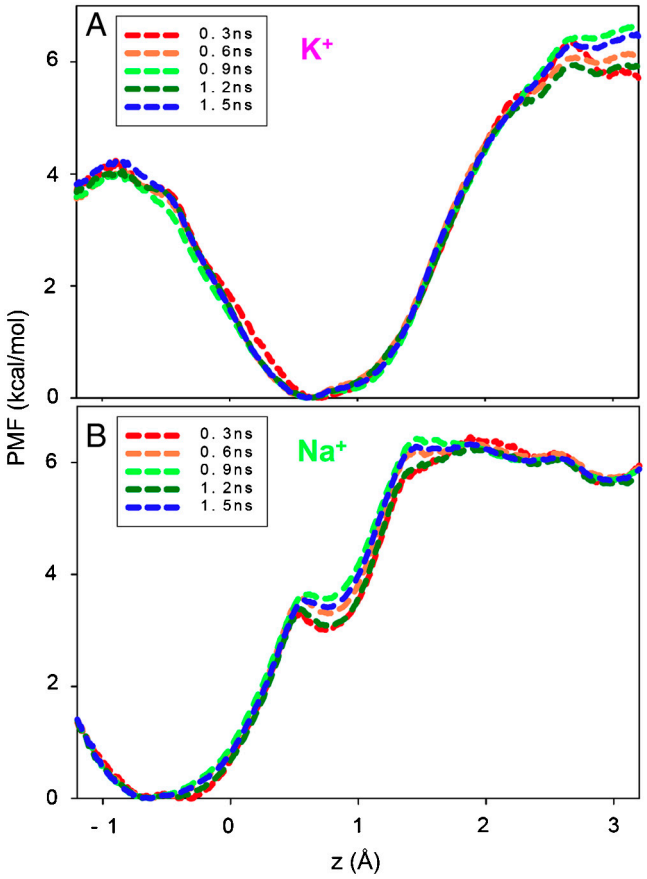

Fig. S2. Convergence and error estimates for free energy profiles: Time convergence for the free energy profiles presented in Fig. 3 of the main text, from 0–1 ns, demonstrating that PMFs have converged to within a fraction of a kcal/mol. Convergence profile of PMFs from 1D US for K^+ (*A*) and Na^+ (*B*), respectively, in the S2 site.

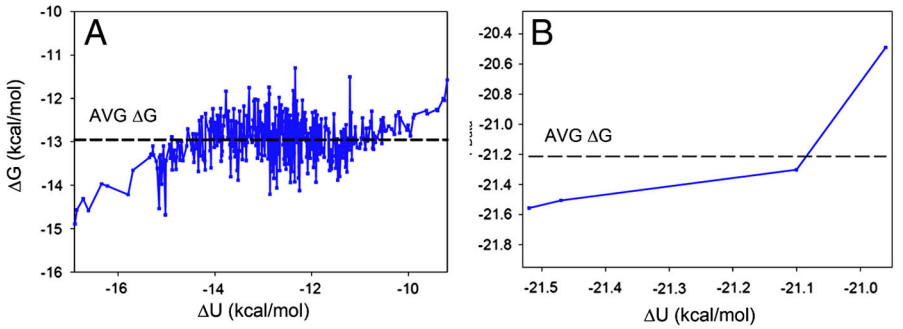

Site FEP	TI	WHAM	BAR-US	BOH-US
Cage (S2)	-13.40± 0.27	-13.10± 0.25	-12.97 ± 0.05	-12.95 ± 0.53
Lower plane (B12)	-21.93± 0.31	-21.80± 0.29	-22.06± 1.23	-21.21± 0.42

Fig. S3. Comparison of FEP and BAR estimates of $\Delta\Delta G$ in individual sites: The free energy differences by BOH-US in the cage of S2 (*A*) and in the plane of S2 (B12) (*B*).

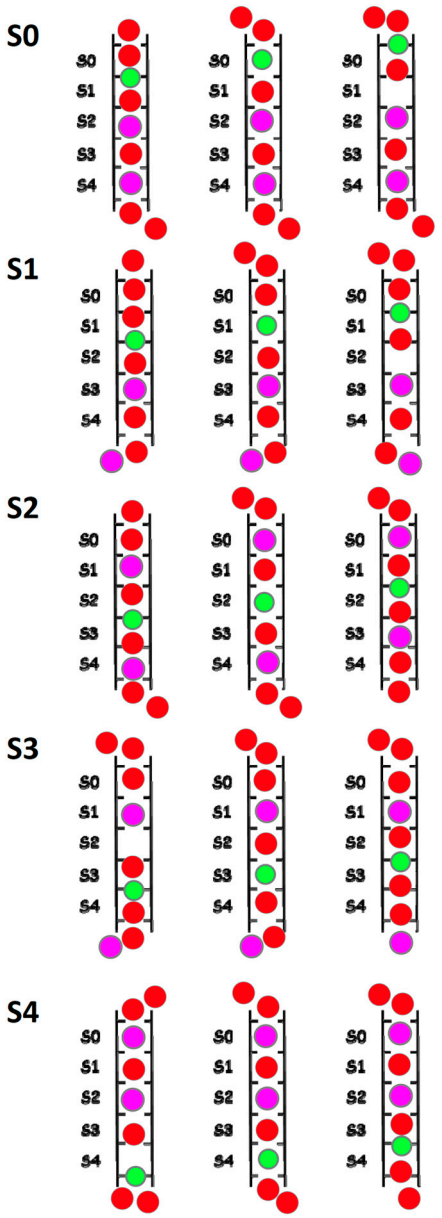

Fig. S4. Schematic illustrating possible consequences for Na^+ movements to plane sites for other ions and water molecules in the selectivity filter. In general, as the ion moves to a plane further from the center of the filter, it creates a void in the single-file column, whereas when it moves to a plane deeper inside the filter, it leads to some compacting of the neighboring water molecule, with different energetic strains, and possible ionic movements.

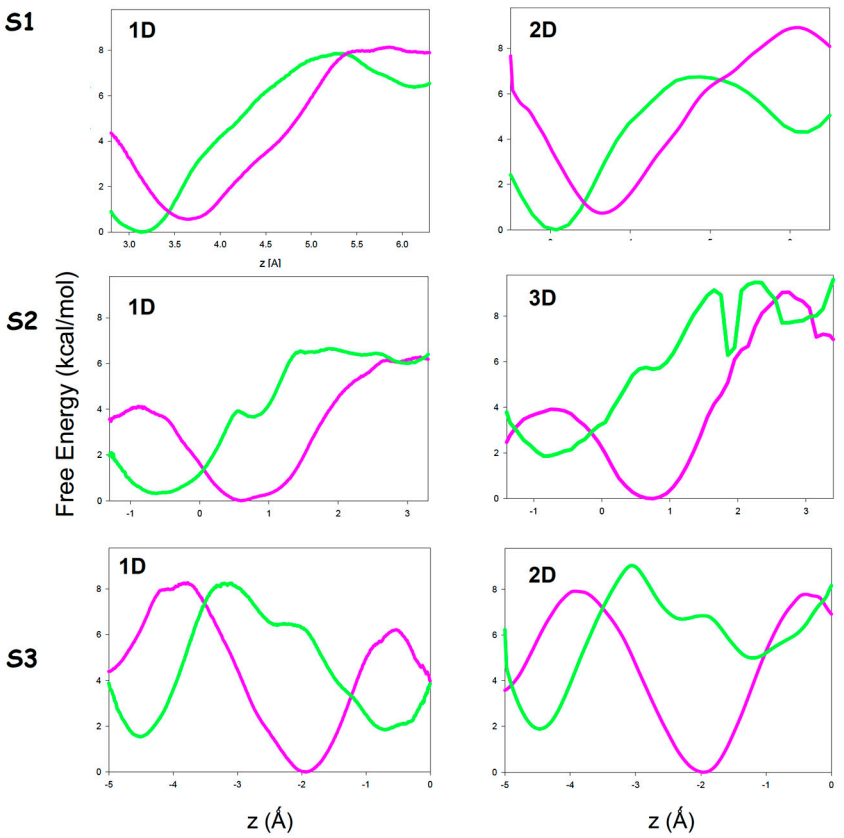

Fig. S5 Comparison of 1D PMFs emerging from 1, 2, and 3-D US.

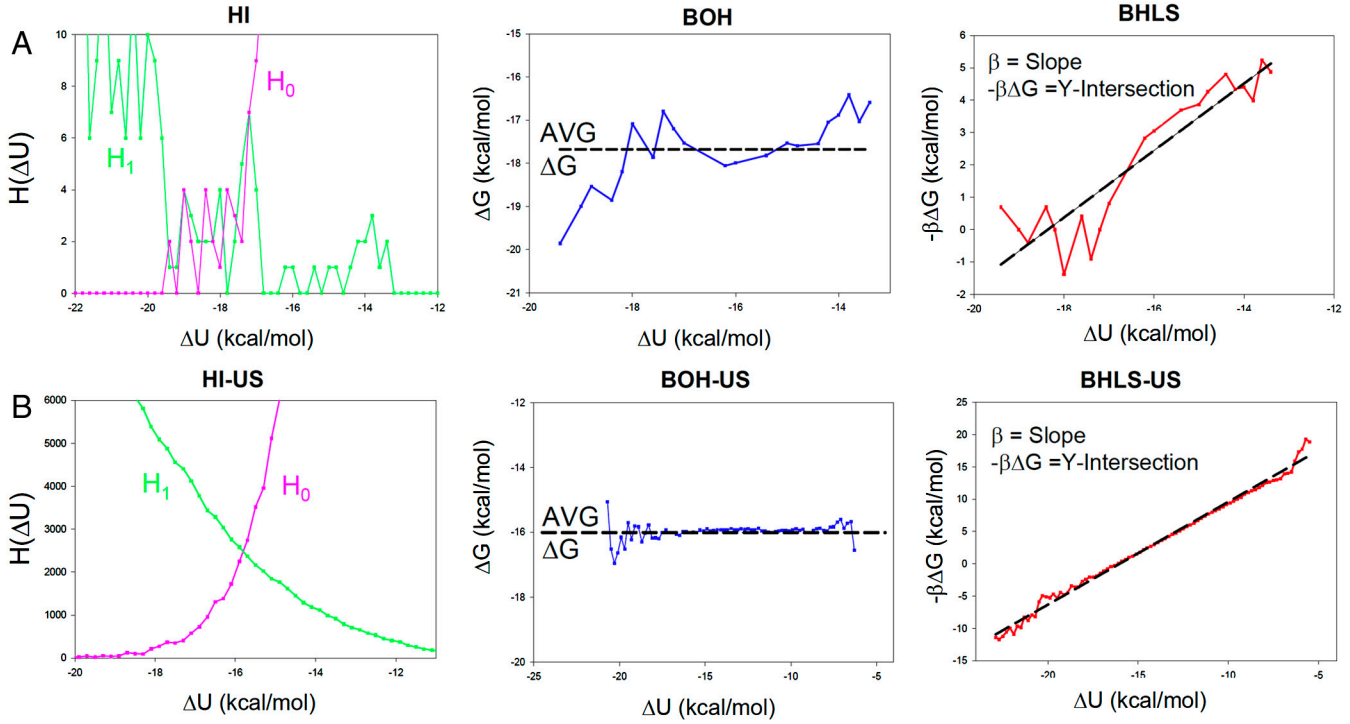

Fig. S6. Comparison of BAR/BOH/BHLS and BAR-US/BOH-US/BULS-US for unconstrained ions: Comparison of free energy differences by three histogram analysis methods across S2 for unconstrained simulations (*A*) (left—HI; center—BOH; right—BHLS) and 3D US simulations (*B*) (HI-US;BOH-US;BHLS-US).

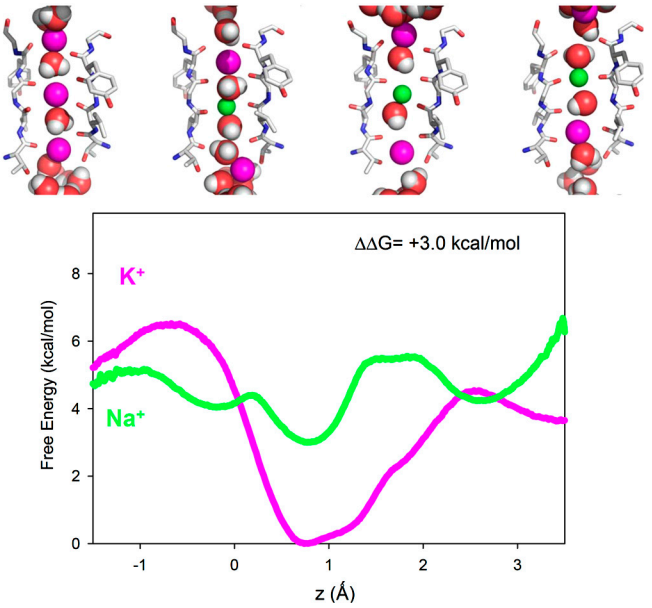

Fig. S7. Nonconducting filter simulations: Representative snapshots of the configurations of ions across S2 sites and corresponding PMFs in the absence of a constraint maintaining a conductive conformation.

Table S1. Free energy perturbation results and ion configuration changes for all simulations: this table is an extended version of Table 1 of the main text

Site	Equilibrated configuration	$\Delta G(K^+ \rightarrow Na^+)$	$\Delta\Delta G(K^+ \rightarrow Na^+)$	
	Before perturbation (K^+)	After perturbation (Na^+)	(kcal/mol)	
Bulk TI	-	-	−18.44 ± 0.02	-
Bulk WHAM	-	-	−18.18 ± 0.02	-
Bulk BAR	-	-	−18.3 ± 0.1	-
Bulk BAR-US*	-	-	−18.38 ± 0.05	**0**
S0 crystal	**S0**(Na^+)/S2(K^+)/S4(K^+)	**S0**(Na^+)/S2(K^+)/S4(K^+)	−16.6 ± 0.3	+1.7 ± 0.3
B01 plane	**B01**(K^+)/S2(K^+)/S4(K^+)	**B01**(Na^+)/S2(K^+)/S4(K^+)	−20.4± 0.9	−2.0 ± 0.1
S0 unconstrained	**S0**(K^+)/S2(K^+)/S4(K^+)	**B01**(Na^+)/S2(K^+)/S4(K^+)	−19.3 ± 0.1	−0.9 ± 0.1
S0 BAR-US-1D	**US-S0**(K^+)/S2(K^+)/S4(K^+)	**US-S0**(Na^+)/S2(K^+)/S4(K^+)	−19.1 ± 0.1	**−0.7 ± 0.1**
S1 cage	**S1**(K^+)/S3(K^+)/Cav(K^+)	**S1**(Na^+)/S3(K^+)/Cav(K^+)	−15.8 ± 0.1	+2.6 ± 0.2
B01 plane	**B01**(K^+)/S3(K^+)/Cav(K^+)	**B01**(Na^+)/S3(K^+)/Cav(K^+)	−19.8 ± 0.3	−1.4 ± 0.3
B12 plane	**B12**(K^+)/S3(K^+)/Cav(K^+)	**B12**(Na^+)/S3(K^+)/Cav(K^+)	−21.2 ± 0.4	−2.8 ± 0.4
S1 unconstrained	**S1**(K^+)/S3(K^+)/Cav(K^+)	**B01**(Na^+)/S3(K^+)/Cav(K^+)	−18.6 ± 0.3	−0.3± 0.3
S1 BAR-US-1D	**US-S1**(K^+)/S3(K^+)/Cav(K^+)	**US-S1**(Na^+)/S3(K^+)/Cav(K^+)	−18.94 ± 0.05	−0.56 ± 0.07
S1 BAR-US-2D	**US-S1**(K^+)/US − S3(K^+)/Cav(K^+)	**US-S1**(Na^+)/US − S3(K^+)/Cav(K^+)	−19.12 ± 0.06	**-0.74 ± 0.07**
S2 cage	S0(K^+)/**S2**(Na^+)/S4(K^+)	S0(K^+)/**S2**(Na^+)/S4(K^+)	−12.97 ± 0.05	+5.42 ± 0.07
B12 plane	S0(K^+)/**B12**(K^+)/S4 ⇌ S3(K^+)	S0(K^+)/**B12**(Na^+)/S3(K^+)	−20.5 ± 2.3	−2.2 ± 0.4
B23 plane	S0(K^+)/**B23**(K^+)/S4(K^+)	S1(K^+)/**B23**(Na^+)/S4 ⇌ Cav(K^+)	−22.0 ± 1.2	−3.7 ± 0.6
S2 unconstrained	S0(K^+)/**S2**(K^+)/S4(K^+)	S1(K^+)/**B23**(Na^+)/S4(K^+)	−17.9 ± 0.3	+0.5 ± 0.3
S2 BAR-US-1D	S0(K^+)/**US-S2**(K^+)/S4(K^+)	S0-S1(K^+)/**US-S2**(Na^+)/S4(K^+)	−18.06 ± 0.04	+0.32 ± 0.06
S2 BAR-US-3D	US-S0(K^+)/**US-S2**(K^+)/US-S4(K^+)	US-S0(K^+)/**US-S2**(Na^+)/US-S4(K^+)	−16.11 ± 0.009	**+2.27** ± 0.05
S3 cage	S1(K^+)/**S3**(K^+)/Cav(K^+)	S1(K^+)/**S3**(Na^+)/Cav(K^+)	−13.42 ± 0.06	+4.96 ± 0.07
B23 plane	S1(K^+)/**B23**(K^+)/Cav(K^+)	S1(K^+)/**B23**(Na^+)/Cav(K^+)	−22.35 ± 0.3	−3.9 ± 0.3
B34 plane	S1(K^+)/**B34**(K^+)/Cav(K^+)	S1(K^+)/**B34**(Na^+)/Cav(K^+)	−21.82± 0.5	−3.4± 0.5
S3 unconstrained	S1(K^+)/**S3**(K^+)/Cav(K^+)	S1(K^+)/**B23**(Na^+)/Cav(K^+)	−16.4 ± 0.4	+2.0 ± 0.4
S3 BAR-US-1D	S1(K^+)/**US-S3**(K^+)/Cav(K^+)	S1(K^+)/**US-S3**(Na^+)/Cav(K^+)	−16.84± 0.06	+1.54 ± 0.07
S3 BAR-US-2D	US-S1(K^+)/**US-S3**(K^+)/Cav(K^+)	US-S1(K^+)/**US-S3**(Na^+)/Cav(K^+)	−16.49 ± 0.05	**+1.89 ± 0.05**
S4 cage	S0(K^+)/S2(K^+)/**S4**(K^+)	S0(K^+)/S2(K^+)/**S4**(Na^+)	−14.41 ± 0.07	+3.97 ± 0.09
B34 plane	S0(K^+)/S2(K^+)/**B34**(K^+)	S0(K^+)/S2(K^+)/**B34**(Na^+)	−23.0±0.4	−4.7 ± 0.4
S4 unconstrained	S0(K^+)/S2(K^+)/**S4**(K^+)	S0(K^+)/S2(K^+)/**B34**(Na^+)	−19.7 ± 0.4	−1.3 ± 0.4
S4 BAR-US-1D	S0(K^+)/S2(K^+)/**US-S4**(K^+)	S0(K^+)/S2(K^+)/**US-S4**(Na^+)	−19.7 ± 0.1	**−1.3± 0.2**

The relative thermodynamic stability of Na^+ compared to K^+, $\Delta G(K^+ \rightarrow Na^+)$, in bulk water and KcsA selectivity filter sites from FEP (TI, WHAM, and BAR), as well as with US (BAR-US) as well as with US (BAR-US). The multiple ion configurations before and after simulations are shown, involving the S0, S1, S2, S3, S4, or cavity crystallographic sites, and B01, B12, B23, or B34 plane sites. All $\Delta G(K^+ \rightarrow Na^+)$ values involving a perturbation in a selectivity filter site were computed using the BAR-US method, except for the unconstrained calculations which were evaluated by BAR. Free energies are expressed relative to bulk water, $\Delta\Delta G(K^+ \rightarrow Na^+)$, using the BAR-US bulk water reference. Errors are standard deviations from nine independent 1ns samples in the bulk case, and are BAR standard deviations in other cases.

*Although the benefit of using US in bulk is additional sampling only.